













RESEARCH ARTICLE | MAY 10 2024

Small multimodal thermometry with detonation-created multi-color centers in detonation nanodiamond

Frederick T.-K. So ; Nene Hariki ; Masaya Nemoto; Alexander I. Shames ; Ming Liu; Akihiko Tsurui; Taro Yoshikawa; Yuto Makino ; Masanao Oho; Masanori Fujiwara ; Ernst David Herbschleb ; Naoya Morioka ; Izuru Ohki ; Masahiro Shirakawa; Ryuji Igarashi ; Masahiro Nishikawa ; Norikazu Mizuochi  



APL Mater. 12, 051102 (2024)
<https://doi.org/10.1063/5.0201154>



APL Energy
Latest Articles Online!

Read Now



Small multimodal thermometry with detonation-created multi-color centers in detonation nanodiamond

Cite as: APL Mater. 12, 051102 (2024); doi: 10.1063/5.0201154

Submitted: 30 January 2024 • Accepted: 5 April 2024 •

Published Online: 10 May 2024



View Online



Export Citation



CrossMark

Frederick T.-K. So,^{1,2} Nene Hariki,¹ Masaya Nemoto,¹ Alexander I. Shames,³ Ming Liu,⁴ Akihiko Tsurui,⁴ Taro Yoshikawa,⁴ Yuto Makino,⁴ Masanao Ohori,¹ Masanori Fujiwara,¹ Ernst David Herbschleb,¹ Naoya Morioka,^{1,5} Izuru Ohki,² Masahiro Shirakawa,^{2,6} Ryuji Igarashi,^{2,7} Masahiro Nishikawa,⁴ and Norikazu Mizuochi^{1,5,a)}

AFFILIATIONS

¹Institute for Chemical Research, Kyoto University, Gokasho, Uji, Kyoto 611-0011, Japan

²Institute for Quantum Life Science, National Institutes for Quantum Science and Technology, Anagawa 4-9-1, Inage-ku, Chiba 263-8555, Japan

³Department of Physics, Ben Gurion University of the Negev, 8410501 Beer-Sheva, Israel

⁴Daicel Corporation, 1239, Shinzaike, Aboshi-ku, Himeji, Hyogo 671-1283, Japan

⁵Center for Spintronics Research Network, Institute for Chemical Research, Kyoto University, Gokasho, Uji, Kyoto 611-0011, Japan

⁶Department of Molecular Engineering, Graduate School of Engineering, Kyoto University, Nishikyo-Ku, Kyoto 615-8510, Japan

⁷School of Life Science and Technology, Tokyo Institute of Technology, Ookayama, Meguro-ku, Tokyo 152-8550, Japan

^{a)} Author to whom correspondence should be addressed: mizuochi@scl.kyoto-u.ac.jp

ABSTRACT

Detonation nanodiamond (DND) is the smallest class of diamond nanocrystal capable of hosting various color centers with a size akin to molecular pores. Their negatively charged nitrogen-vacancy center (NV^-) is a versatile tool for sensing a wide range of physical and even chemical parameters at the nanoscale. The NV^- is, therefore, attracting interest as the smallest quantum sensor in biological research. Nonetheless, recent NV^- enhancement in DND has yet to yield sufficient fluorescence per particle, leading to efforts to incorporate other group-IV color centers into DND. An example is adding a silicon dopant to the explosive mixture to create negatively charged silicon-vacancy centers (SiV^-). In this paper, we report on efficient observation ($\sim 50\%$ of randomly selected spots) of the characteristic optically detected magnetic resonance (ODMR) NV^- signal in silicon-doped DND (Si-DND) subjected to boiling acid surface cleaning. The NV^- concentration is estimated by continuous-wave electron spin resonance spectroscopy to be 0.35 ppm without the NV^- enrichment process. A temperature sensitivity of $0.36 \text{ K}/\sqrt{\text{Hz}}$ in an NV^- ensemble inside an aggregate of Si-DND is achieved via the ODMR-based technique. Transmission electron microscopy survey reveals that the Si-DNDs core sizes are $\sim 11.2 \text{ nm}$, the smallest among the nanodiamond's temperature sensitivity studies. Furthermore, temperature sensing using both SiV^- (all-optical technique) and NV^- (ODMR-based technique) in the same confocal volume is demonstrated, showing Si-DND's multimodal temperature sensing capability. The results of the study thereby pave a path for multi-color and multimodal biosensors and for decoupling the detected electrical field and temperature effects on the NV^- center.

© 2024 Author(s). All article content, except where otherwise noted, is licensed under a Creative Commons Attribution (CC BY) license (<https://creativecommons.org/licenses/by/4.0/>). <https://doi.org/10.1063/5.0201154>

I. INTRODUCTION

The negatively charged nitrogen-vacancy center (NV^-) in diamond¹ is a fascinating quantum defect with a long spin coherence time at ambient conditions² and has been a topic of great interest in quantum information science and technology.³ In particular, it has been extensively studied in the field of quantum sensing because of its high sensitivity to temperature,^{4,5} magnetic field,⁶ and electric field.⁷ The discovery that diamond nanoparticles exhibit low cytotoxicity has led to the transfer of these quantum sensing techniques into biology in recent years, extending toward biomedical applications⁸ such as detecting radicals at the subcellular level,⁹ observing movements of proteins at the molecular level,⁶ enhancing the detection sensitivity of the HIV,¹⁰ and measuring thermal conductivity at the subcellular level,¹¹ etc. Among these applications, temperature sensing at the subcellular level has attracted significant interest because the temperature in living cells reflects thermodynamics and plays an important role in regulating cell activities.^{12–14} In particular, researchers have demonstrated that the membrane vesicles in cells can be modulated by temperature.¹⁵ However, the common bio-probe used to investigate these phenomena often suffers from photobleaching or high cytotoxicity.¹⁶ The photostable and biocompatible diamond probe, therefore, represents a promising tool for long-term monitoring of cellular activities,¹⁷ notably millikelvin sensitivity in living cells.⁵

Nevertheless, the biological utility of the diamond sensors faces a dilemma rooted in particle size,¹⁸ where larger particles possess adequate brightness because of their higher concentration of color centers, yet their size restricts access to cell organelles.¹⁹ Conversely, smaller particles should allow better penetration,²⁰ but often at the expense of reduced luminosity because of a lower number of color centers.²¹ These challenges have, therefore, motivated the development of ultrasmall, yet luminous, diamond sensors. Among other synthesis methods available for fabricating nano-sized diamond sensors, the synthesis of detonation nanodiamond (DND) is a promising approach to creating ultrasmall sensors by bottom-up synthesis via an explosion (trinitrotoluene and hexogen) inside a metallic chamber, commonly known as dynamic detonation synthesis. The resultant DND has the advantage of a nitrogen content up to 2%–3% in atomic ratio and a substitutional nitrogen (N_S) concentration typically estimated at 1000 ppm.^{21–23} The abundance of N_S , therefore, provides sufficient precursor to achieve the high concentration of NV^- necessary for highly sensitive quantum sensing applications.²⁴ More importantly, DND particles have an ultrasmall size (typically 5 nm), a narrow size distribution, and a spherical shape,²⁵ making them ideal for non-invasive in-cell investigations.

Recent advances in DND-based sensors have led to the efficient creation of negatively charged silicon-vacancy centers (SiV^-) and negatively charged germanium-vacancy centers²⁵ (GeV^-) in DND via the introduction of triphenylsilanol or tetraphenylgermane^{26,27} into the explosive starting materials. This synthesis activates the SiV^- and GeV^- without electron irradiation or annealing inside ultrasmall diamond particles suitable for sub-organelle investigation,^{28,29} greatly simplifying the process and reducing the production cost. Despite the success in synthesizing color centers other than NV^- , previous attempts to observe optically detected magnetic resonance (ODMR) for NV^- -centers in silicon-

doped DND have been unsuccessful.³⁰ Although the temperature-dependence shift in the zero-phonon-line (ZPL) of SiV^- in the near-infrared region has been an important subject in enabling deeper *in vivo* studies,^{31–33} the lack of NV^- ODMR signals presents a critical shortcoming because the unobservable ODMR signal for SiV^- at ambient conditions has limited its role to all-optical thermometry currently. However, the long spin coherence time for NV^- enables the sensing of a wide range of parameters at ambient conditions. The superior quantum properties of NV^- also ensure a greater sensitivity compared with the all-optical method,²⁹ where the temperature sensitivity can be enhanced to $5 \text{ mK}/\sqrt{\text{Hz}}$ in a single NV^- inside bulk diamond. However, this sensitivity is reduced to $130 \text{ mK}/\sqrt{\text{Hz}}$ in 50 nm nanodiamonds, mainly because of the deteriorated spin coherence time for NV^- in smaller diamonds.⁴ To shed light on how small diamonds can be fabricated without losing the sensitivity necessary for their application, we conduct a material investigation on Si-DNDs, followed by temperature sensing with ODMR techniques to evaluate their temperature sensitivity as one of the representative characteristics.

II. EXPERIMENTAL DETAILS

The silicon-doped detonation diamond particles are prepared using the previously reported protocol,³⁴ involving a mixed explosive (60 wt. % TNT, 40 wt. % RDX) doped with silicon dopant (triphenylsilanol), whereas the silicon dopant is 1% of the mixed explosive mass. A separate batch of DND is also prepared using the same procedure but without the silicon dopant to investigate the effect of silicon doping on NV^- formation. The detonation is conducted in a CO_2 atmosphere. The Si-DND is then air-oxidized in O_2/N_2 (4:96 vol. %) at $570^\circ C$ for 2 h.³⁴ Drop casting of both DND samples onto cover glass yields only an extremely low contrast continuous-wave optically detected magnetic resonance peak (cw-ODMR) peak (0.4% maximum) in confocal microscopy and no observable 637 nm ZPL peak in photoluminescence spectroscopy.²⁵ To investigate whether NV^- is indeed absent or if other possible factors hinder the cw-ODMR signal observation, continuous-wave electron spin resonance (cw-ESR) is employed to detect the NV^- forbidden transition signals.^{21,35,36} The cw-ESR spectra of Si-DND (34.7 mg) are recorded using an X-band ($\nu \approx 9.85 \text{ GHz}$) ELEXSYS E 500 spectrometer manufactured by Bruker (USA) and equipped with an ELEXSYS super high sensitivity probe head (ER 4122SHQE).²¹ After successful confirmation of the NV^- presence, an intensive boiling acid treatment ($HNO_3:H_2SO_4$, 1:3, v/v) is performed at $130^\circ C$ for 3 days for both DND samples to remove surface impurities^{21,24} for reliable NV^- quantification via the integration of the forbidden transition signal intensity.^{35,37} The resultant surface-cleaned samples are hereafter referred to as Si-DND and nSi-DND, representing silicon-doped DND and non-silicon-doped DND, respectively. Transmission electron microscopy (TEM) is used to survey the particle size of the Si-DND and nSi-DND. Optical evaluations are performed with a home-built microscope and an evaporated powder sample that has been reported elsewhere.^{25,30} The microscope includes a 532 nm laser and a $100\times$ oil-immersion lens (numerical aperture of 1.45) attached to a piezo stage, with a thin copper wire (diameter of 30 μm) attached to the sample surface to introduce microwaves for spin manipulation. A thermistor is embedded in the copper plate to provide a reference temperature reading. The removal of

surface impurities leads to ~50% of the randomly selected bright spots displaying the signature NV^- 's cw-ODMR peak at 2.87 GHz, which is used for temperature sensing with an evaluation of their temperature sensitivity. Finally, temperature sensing with NV^- and SiV^- in a single bright spot is performed to demonstrate the feasibility of multimodal temperature sensing protocols with Si-DND sensors.

III. RESULTS AND DISCUSSION

A. Materials characterization

Si-DND and nSi-DND are examined using electron spin resonance (ESR) spectroscopy [Fig. 1(a)], where the NV^- forbidden transition peak is located at ~168 mT and the divacancy peak is located at ~176 mT.³⁶ The spectra are calibrated using a DND sample with a known NV^- concentration.^{21,24} This sample also serves as a standard for estimating the NV^- concentration in both Si-DND and nSi-DND, both of which are determined to be 0.35 ± 0.05 ppm. NV^- can be quantified using a half-field measurement because of its $S = 1$ spin property,³⁵ whereas SiV^- can be quantified using a main-field measurement due to its spin $S = 1/2$.³⁸ Nonetheless, the very high concentration of $S = 1$ electron spins in DND, including the neutral N_S and isolated dangling bonds, creates a broad signal that hinders SiV^- 's quantification.^{21,38,39}

The removal of surface impurities not only allows a reliable estimation of NV^- via ESR but also contributes to the observation of the NV^- ODMR signal at 2.87 GHz [Fig. 1(b)]. Before the boiling acid treatment, only an extremely low-contrast ODMR peak, with a maximum of 0.4%, is detected for the Si-DND [Fig. 1(b), black circles]. By contrast, the post-treatment Si-DND often exhibited greater than 10% ODMR contrast [Fig. 1(b), blue circles]. To gain insight into the particle size for both samples, we analyze a series of TEM images. Representative images of the Si-DND and nSi-DND samples are depicted in Figs. 1(c) and 1(e), respectively. The analysis, which focused on the largest diameter of the particle core and encompassed 212 Si-DND and 209 nSi-DND particles, summarizes the revealed size distributions in Figs. 1(d) and 1(f), respectively. The average particle core size of Si-DND particles is 11.2 nm, with a standard deviation of 3.0 nm [Fig. 1(d)] (see Fig. S1 for TEM analysis in the supplementary material). The average particle core size of nSi-DND particles is 10.9 nm, with a standard deviation of 3.1 nm, which is almost the same as those for the Si-DND particles [Fig. 1(f)]. This particle size (11.2 nm), along with the NV^- concentration from the ESR spectrum (0.35 ppm), gives an average NV^- concentration of 1 NV^- per 22 Si-DND particles. The enhancement in ODMR contrast may be attributed to the removal of non-diamond carbon often found on the surface of DND, which may exhibit bright fluorescence and substantially reduce the ODMR contrast for NV^- in DND.⁴⁰ The percentage of bright spots showing an ODMR signal is examined for randomly selected bright spots in Si-DND and nSi-DND samples. In this examination, ~50% of the bright spots in Si-DND (39 of 80–90 measured spots) exhibited ODMR signals, while the percentage for nSi-DND is similar (53 of 100–110 measured spots). This result represents a substantial improvement after surface cleaning and an enhancement relative

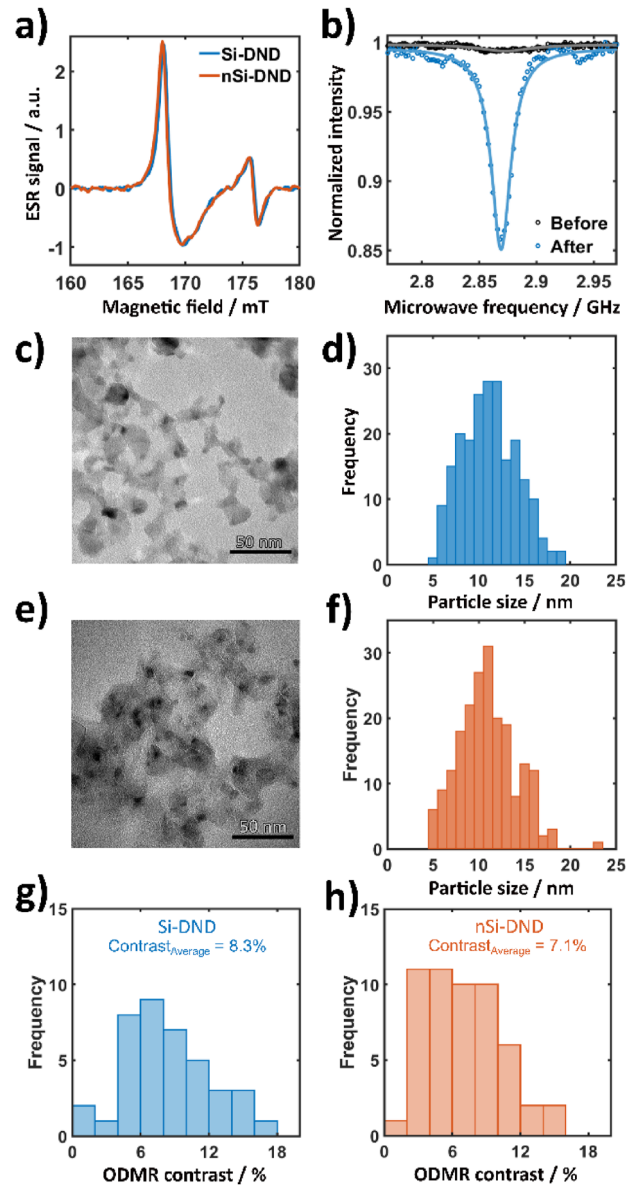


FIG. 1. (a) Half-field electron spin resonance spectra of Si-DND (blue line) and nSi-DND (orange line), as acquired using an X-band ($\nu \approx 9.85$ GHz) spectrometer. The spectra are background corrected and calibrated with a nanodiamond sample with a known NV^- concentration. The NV^- forbidden transition peak ($\Delta m_S = 2$) is located at ~168 mT, while the divacancy peak is located at ~176 mT. (b) Representative ODMR spectra of Si-DND before (black circles) and after (blue circles) boiling acid treatment; a high ODMR contrast (~15%, blue line) is detected at 2.87 GHz after the boiling acid treatment, whereas only a low ODMR contrast signal (~0.4%, gray line) is detected before this treatment. (c) Representative TEM image of Si-DND aggregates. (d) TEM particle size distribution analysis of 212 Si-DND particles. (e) Representative TEM image of nSi-DND aggregates. (f) TEM particle size distribution analysis of 209 nSi-DND particles. (g) Summary histogram of ODMR contrast measured in 39 randomly selected spots in Si-DND. (h) Summary histogram of ODMR contrast measured in 53 randomly selected spots in nSi-DND.

to the percentage previously reported for DND, where only 16.5% (51 of 309 spots) of the fluorescence spots displayed ODMR signals.¹⁸ This improvement, however, can be attributed to multiple factors, including differences in the surface modification methods (carboxyl terminated vs hydroxyl terminated), variations in particle size (11.2 vs 5 nm), differences in the NV⁻ concentration (0.35 vs 0.11 ppm²¹), and an uncontrolled number of DND particles inside the observed aggregate. Figures 1(g) and 1(h) show a summary histogram of the ODMR contrasts in Si-DND and nSi-DND, respectively, revealing that both samples exhibit a similar high contrast in ODMR measurements. Given the lack of a significant difference between the two samples, we primarily investigated Si-DND in the present study.

B. Temperature sensitivity of NV⁻

To apply these ultrasmall Si-DND particles to nanoscale thermometry, ten bright spots of NV⁻ are selected for temperature sensing using the cw-ODMR method (see Fig. S2 and Table S1 in the supplementary material). All of the ODMR spectra show a temperature-dependent shift when the temperature of the sample holder is increased using a thermal plate together with a lens heater for the objective lens. The PL spectra and ODMR spectra of all ten spots can be found in the supplementary material Fig. S3. Representative data collected using one of the ten bright spots are presented in Fig. 2. As shown by the PL spectrum in Fig. 2(a), the NV⁻ ZPL at ~637 nm and the NV⁰ ZPL at ~575 nm can be recognized. The ODMR spectra collected at 295 and 313 K show a distinctive temperature-dependent shift in the zero-field splitting frequency (D) [Fig. 2(b)]. To calculate the D value from the spectrum, we fit the data with a double Lorentzian function and average the two centers from the two Lorentzian curves.^{11,29} The resultant D value with the combined standard error at different temperatures is then plotted against the temperature reading of the thermistor [Fig. 2(c)]. To extract the dD/dT value, the data points are fitted linearly, resulting in a dD/dT value of -72.2 ± 1.3 kHz/K. The ten different NV⁻ fluorescence spots have an average dD/dT value of -71.2 kHz/K, which closely agrees with the commonly reported dD/dT values commonly reported for other diamond samples.^{2,5,17,41,42} The dD/dT values of the ten spots can be found in supplementary material Fig. S4.

The temperature sensitivity of the NV⁻ ensemble is proportional to $1/\sqrt{t_{\text{int}}}$, where t_{int} is the integration time. All 10 NV⁻ spots investigated are further examined to find the temperature sensitivity. The concept of the measurement is inspired by alternating current magnetic field sensitivity measurements.² A working point of maximum gradient is chosen from the double Lorentzian fitting and used for temperature sensitivity evaluation. The fluorescence intensity trace under continuous-wave microwave irradiation at the steepest slope frequency is then recorded at different t_{int} from 0.003 to 2 s using a single photon detector. Next, the standard deviation of the fluorescence intensity fluctuation is divided by the obtained maximum gradient, translating into the fluctuation in the microwave resonance frequency. This standard deviation is further divided

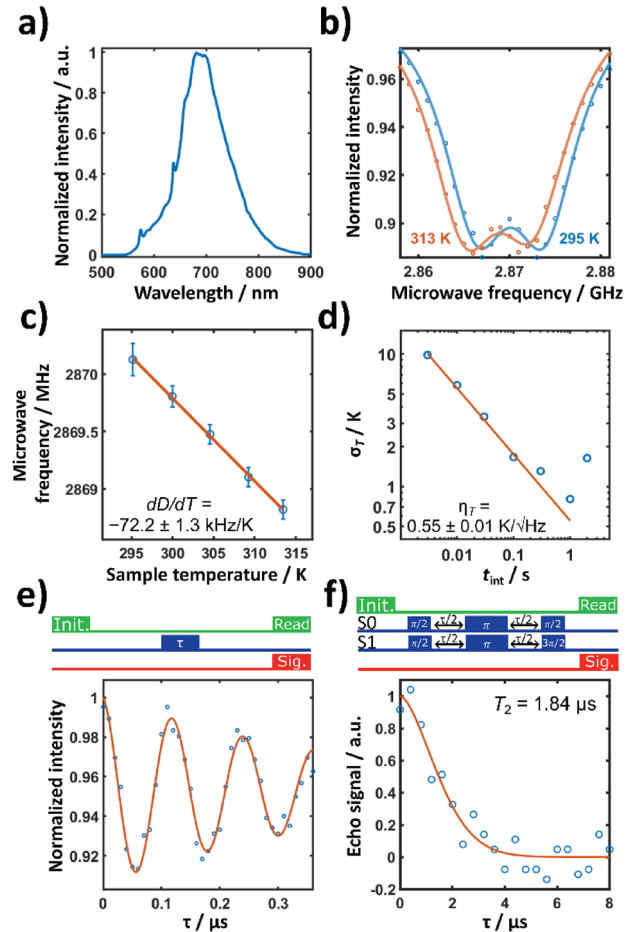


FIG. 2. Spectra of a representative NV⁻ spot found inside the Si-DND aggregate. (a) PL spectrum of the spot used for temperature sensing. (b) ODMR spectra recorded at 295 K (blue circles) and 313 K (orange circles) and fit with double Lorentzian functions (blue and orange lines). (c) The zero-field splitting center (D) of ODMR as a function of sample temperature, calculated as the average of the peaks of the two Lorentzian functions. The peak sensitivity to temperature (dD/dT) is obtained by a linear fit (orange line) to the calculated D data (blue circles with error bars). The individual error bar is the combined standard error from the two Lorentzian fittings on the corresponding ODMR spectrum. (d) Standard deviation of temperature uncertainty (σ_T) vs time of integration (t_{int}) measured at room temperature 295 K (blue circles), fit with $\sigma_T = \eta/\sqrt{t_{\text{int}}}$, where η is the temperature sensitivity, giving a η of 0.55 ± 0.01 K/ $\sqrt{\text{Hz}}$. (e) Rabi oscillation of the $m_S = 0 \rightarrow m_S = -1$ transition. (f) Hahn echo (T_2) measurement ($\frac{S_0 - S_1}{S_0 + S_1}$) of the representative spot. The collected fluorescence signal is plotted and fitted with $e^{-\left(\frac{\tau}{T_2}\right)^n}$. The resulting T_2 value is determined to be 1.84 μs . All spectra are collected from the same fluorescence spot. Spectra from (a) to (d) are collected under a zero magnetic field, whereas spectra from (e) to (f) are collected under an external static magnetic field. The sequences above the plots (e) and (f) show the applied pulse sequences. Green, blue, and red blocks symbolize optical excitation pulses (laser pulses), microwave radiation pulses, and fluorescence readout pulses, respectively.

by the corresponding dD/dT value from ODMR measurements [Fig. 2(c)], giving the uncertainty in temperature (σ_T) [Fig. 2(d)]. The data points are fitted with $\sigma_T = \eta_T/\sqrt{I_{\text{int}}}$, where η is the temperature sensitivity, giving a sensitivity η_T of 1.74 ± 0.04 K/ $\sqrt{\text{Hz}}$ for the spot in Fig. 2. To mitigate saturation of the avalanche photodiode (APD) during data acquisition, a neutral density filter with an optical density of 1.0 is employed before the APD, reducing the fluorescence intensity by a factor of 10. Within the short accumulation time, the measurement accuracy is limited by the shot-noise ($1/\sqrt{N_{\text{ph}}}$), thus the sensitivity without a neutral density filter is estimated to be 0.55 ± 0.01 K/ $\sqrt{\text{Hz}}$ for the NV⁻ ensemble within the Si-DND aggregate [Fig. 2(d)]. To estimate the sensitivity of a single NV⁻, the equation $\eta_{\text{ensemble}} = \eta_{\text{single}}/\sqrt{N}$ is applied, where η_{ensemble} is the sensitivity of NV⁻ ensembles, η_{single} is the sensitivity of a single NV⁻, and N is the estimated number of NV⁻ centers within the confocal volume. This estimated number of NVs⁻ is derived from the fluorescence intensity of a single NV⁻ in bulk diamond measured using the same setup. The spot depicted in Fig. 2 is estimated to contain 23 NVs⁻. Hence, the sensitivity of a single NV⁻ is determined to be $0.55 \pm 0.01 \times \sqrt{23} = 2.64 \pm 0.06$ K/ $\sqrt{\text{Hz}}$. All single NV⁻ estimations can be found in supplementary material Fig. S5.

To investigate the spin properties of NV⁻, Rabi oscillation and spin Hahn echo measurements are conducted in the presence of an external magnetic field applied by a permanent magnet. The results of these measurements are presented in Figs. 2(e) and 2(f). The spin coherence time (T_2) measured from Hahn echo experiments is found to be 1.84 μs , which is consistent with those commonly reported for DND.¹⁸ According to a previous study, T_2 of an ensemble of NV⁻ scales with the N_S concentration; thus, the observed T_2 in Si-DND may suggest a local N_S concentration of 100 ppm in the vicinity of the NV⁻.⁴³ This N_S concentration estimation contradicts the ~ 1000 ppm of N_S estimated by ESR.²¹ However, it is important to note that the high concentration of paramagnetic defects (N_S and dangling bonds) in DND may lead to a different interaction mechanism between the NV⁻ and a paramagnetic spin bath than that in bulk diamond. The small particle size of the Si-DND (11.2 nm) also suggests the near-surface NV⁻ exposed to air is not subjected to the N_S decoherence factor, which we attribute to the differences between the two N_S concentration estimations.

The experimental procedures depicted in Figs. 2(b)–2(d) are replicated across ten distinct spots dominated by NV⁻. The resultant data yield an average ensemble NV⁻ sensitivity of 0.74 K/ $\sqrt{\text{Hz}}$. Similarly, the average estimated sensitivity for a single NV⁻ is determined to be 4.14 K/ $\sqrt{\text{Hz}}$. Among these measurements, the highest temperature sensitivity for an NV⁻ ensemble in a Si-DND aggregate is 0.36 ± 0.01 K/ $\sqrt{\text{Hz}}$. For the estimated single NV⁻ sensitivity, the highest sensitivity observed is 2.64 ± 0.06 K/ $\sqrt{\text{Hz}}$ (obtained from Fig. 2). These values, however, have yet to reach the sensitivity level of 0.13 K/ $\sqrt{\text{Hz}}$ reported for 50 nm single-crystalline high-pressure-high temperature (HPHT) nanodiamonds,⁴ due to the reasons described below.

It is critical to recognize that the sensitivity values reported for Si-DND represent a basic level of performance. Substantially

higher sensitivity could potentially be achieved using sophisticated sequences such as D -Ramsey to mitigate quasistatic noise.⁴ Nonetheless, these techniques often necessitate the separation of $m_S = \pm 1$ states using an external magnetic field or strain.^{4,44} In our case, multiple Si-DND particles are randomly aggregated on the surface of a cover glass, resulting in NV⁻ centers with random orientations, as opposed to the four possible orientations observed in larger diamond structures. Therefore, the aggregated Si-DND often encompasses multiple NVs⁻ with more than four orientations, leading to the emergence of multiple low-contrast peaks in the spectrum upon the application of an external magnetic field. Although it has been demonstrated that the thermal echo can be applied at zero magnetic field,⁴⁴ this technique relies heavily on a resolvable Rabi oscillation, whereas the multiple NV⁻ with random orientation in Si-DND often leads to unresolvable Rabi oscillations at zero magnetic field. These complexities hinder the effective implementation of the D -Ramsey sequence or thermal echo sequence in the current experiment.^{4,44} In common biological measurements involving NV⁻, in particular, the resonance frequencies and π pulse durations can drastically change as a result of the movement and rotation of the nanodiamond in the dynamic environment.⁶ Meanwhile, the cw-ODMR is generally less affected by these parameters, providing reliable measurements without the complexity of maintaining precise control. The cw-ODMR is, therefore, chosen as the method of study in the present work.

Nevertheless, the specific fluorescence spot depicted in Fig. 2 is estimated to contain ~ 23 NVs⁻. This estimation, when combined with the average number of NV⁻ per particle as determined from ESR data (1 NV⁻ per 22 Si-DND particles) presented in Figs. 1(a) and 1(d), suggests that the Si-DND aggregate (0.55 ± 0.01 K/ $\sqrt{\text{Hz}}$) depicted in Fig. 2(d) is ~ 90 nm in size. In addition, the sensitivity of the NV⁻ is fundamentally linked to the T_2^* coherence time, which exhibits an inverse relationship with the ODMR linewidth. From the perspective of material engineering, DND exhibits distinct material properties in comparison to conventional HPHT diamonds. Notably, during the dynamic detonation synthesis process, a large number of impurities are incorporated into DND particles,^{22,23} leading to the formation of a high concentration of paramagnetic defects, including neutral N_S ²¹ and divacancies [Fig. 1(a)]. Such substantially reduces the coherence time of the NV⁻, thereby constraining their individual temperature sensitivity. Moreover, the ultrasmall particle size of DND, as depicted in Figs. 1(c) and 1(d), implies that the observed NV⁻ are proximal to the particle surface. This proximity likely subjects them to additional decoherence factors, further limiting their sensitivity.^{45–47} These surface-related effects, combined with the intrinsic noisy environment of the DND core, collectively contribute to the reduced coherence time and, hence, to the decreased sensitivity of individual NV⁻ centers. Despite these challenges, DND offers a unique advantage in that the substantial ten-fold increase in the N_S content within DND serves as an abundant source for the formation of NV⁻ in ultrasmall nanodiamonds. Consequently, this heightened density of NV⁻ might effectively counterbalance the reduced sensitivity observed in individual NV⁻, thereby conferring a considerable advantage in terms of overall sensitivity per particle.

C. Temperature sensing with NV^- and SiV^-

The NV^- has diverse sensing applications but requires spin manipulation with microwaves at a frequency of ~ 2.87 GHz. On the contrary, SiV^- requires only laser excitation and PL spectroscopy to read out the ZPL position. The application of microwaves in biological measurements can be difficult because of the absorption by water in biological samples, which introduces artifacts in temperature sensing in cells over time during long-term measurements.²⁹ Hence, it would be ideal to have both color centers inside these ultrasmall diamond sensors to accommodate different needs under various circumstances, such as switching between only temperature sensing mode with SiV^- and quantum sensing mode with NV^- 's ODMR-based technique. This can be realized in two potential cases: the first involves the co-localization of the two types of defects within a single crystal, while the second case concerns an aggregated DND configuration, where different defects are present across multiple crystals. The occurrence of the first case depends on the probability of defect formation, whereas the second case, an aggregated DND with varied defects, is more likely in our current experimental setup. To realize such a multimodal measurement, temperature sensing with both SiV^- and NV^- is demonstrated in Fig. 3. A spot containing a balanced NV^- and SiV^- fluorescence ratio is used for demonstration, illustrated by its PL spectrum in Fig. 3(b), with the ZPLs of NV^- (~ 637 nm) and SiV^- (~ 737 nm) visible in the spectrum. In Fig. 3(c), the cw-ODMR spectra at 295 and 313 K are plotted and fitted with double Lorentzian curves, showing a distinctive temperature-dependent shift. In Fig. 3(d), the D values are plotted against the sample temperature between 295 and 313 K, and the linear fitting of the data point displays a dD/dT value of -81.4 ± 9.1 kHz/K. Meanwhile, the ZPL of SiV^- also displays a shift in the same temperature range; the ZPL at 300 and 313 K are plotted in Fig. 3(e) and fitted with the Lorentzian function and Gaussian function. Apart from the ZPL peak shifting, the fluorescence intensity also substantially decreases when the temperature increases. The peak position of the fitting at different temperatures is plotted in Fig. 3(f) and displays a linear shift of 0.014 ± 0.002 nm/K. Both shifts agree with the reported values found for NV^- ^{4,17,29} and SiV^- ^{30,32,48} in bulk diamond and DNDs, demonstrating that the temperature is indeed detected by the two different types of color centers in the same confocal volume. However, it is not possible to determine whether these two color centers coexist in a single particle. It is unclear because the particle size (11.2 nm) is much smaller than the resolution (full-width at half-maximum of ~ 300 nm) of the confocal microscope.

This simultaneous presence of NV^- and SiV^- centers dedicated to temperature sensing within the same confocal volume potentially expands the versatility of the NV^- toolbox. The zero-field splitting parameter D in NV^- is influenced by both the temperature T and the axial electric field. The NV^- is incapable of distinguishing the shifts from the axial electric field⁷ and temperature from the environment because they shift the zero-field splitting in the same manner. The existence of SiV^- solely detecting the temperature in the same location provides an invaluable tool for distinguishing between temperature-induced shifts and axial electric field-induced shifts using the combined data from both SiV^- and NV^- centers. Notably, the ODMR contrast increases with increasing temperature, contradicting previous reports of reduced ODMR con-

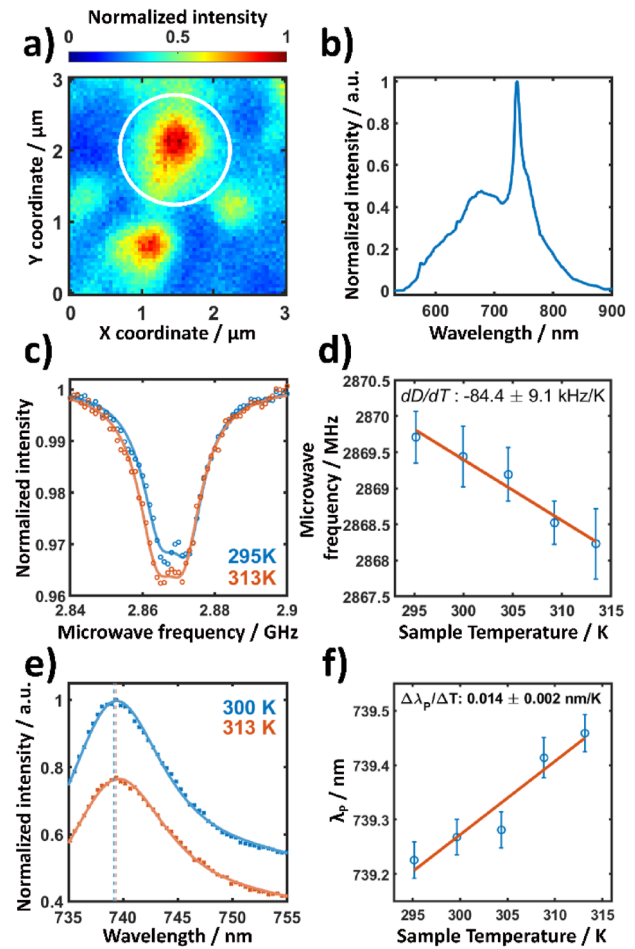


FIG. 3. (a) Confocal image of a spot in Si-DND aggregates containing both NV^- and SiV^- (indicated by a white circle). (b) The PL spectrum of the highlighted spot in (a), with the NV^- (~ 637 nm) and SiV^- (~ 737 nm) zero phonon lines (ZPL) visible in the spectrum. (c) cw-ODMR spectrum of the NV^- , fitted using double Lorentzian curves. The spectrum in blue is recorded at 300 K, whereas that in orange is recorded at 313 K; the orange spectrum displays an increase in contrast upon the increase in temperature. (d) The ODMR center as a function of temperature, with the D values calculated using the average of the two centers in double Lorentzian fitting and the error bar from combining the standard error of the two centers from fitting; a linear regression is applied to experimental data to determine the dD/dT coefficient, which is -84.4 ± 9.1 kHz/K. (e) Comparative PL spectra of the SiV^- ZPL at two temperatures: 300 K (blue dots) and 313 K (orange dots). The spectra are modeled using a Lorentzian function for the SiV^- ZPL and a Gaussian function for the associated SiV^- phonon sideband. (f) ZPL peak wavelengths (λ_p , blue circles) and their standard errors (blue error bars) of SiV^- as a function of sample temperature. The peak sensitivity to temperature ($\Delta\lambda_p/\Delta T$) is obtained by a line fit (orange line) to the experimental data (blue circles).

trast with increasing temperature.^{49,50} This increase of the ODMR contrast is, however, attributable to the reduced fluorescence intensity of SiV^- at elevated temperatures,^{30,48,50} as shown in Fig. 3(e). The SiV^- fluorescence serves as background fluorescence during the ODMR measurement. As the temperature increases, this back-

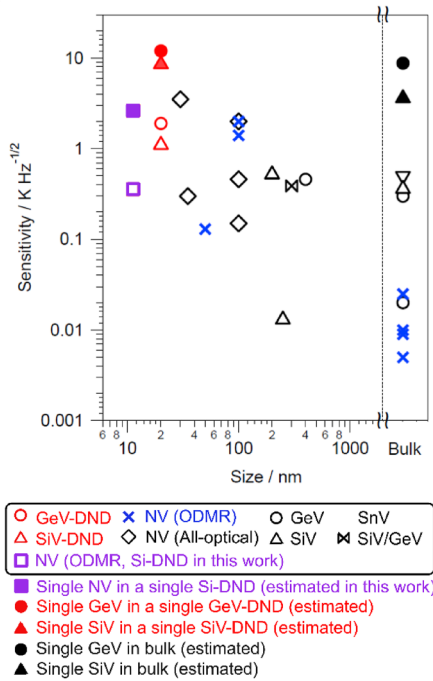


FIG. 4. Plots of diamond core sizes and temperature sensitivities using data acquired in the present study and data from the literature. Red markers are the sensitivity values reported previously by our group, and the purple markers are the sensitivity values obtained in the present work. The hollow purple square shows the best cw-ODMR temperature sensitivity obtained from an ensemble of NV⁻ in our Si-DND aggregate, while the filled purple square shows the best cw-ODMR temperature sensitivity from a single NV⁻ (estimated) in our Si-DND, and the filled purple square shows the result of the best cw-ODMR temperature sensitivity from a single NV⁻ (estimated) in our Si-DND. The red hollow circle shows the result of GeV⁻ in GeV-DND, and the filled red circle is the corresponding estimated single GeV⁻ in GeV-DND.²⁵ The red hollow triangle shows the corresponding temperature sensitivity of SiV⁻ in SiV-DND, and the red filled triangle is the corresponding estimated single SiV⁻ in Si-DND.³⁰ The blue crosses show NV⁻ thermometries based on ODMR techniques (cw-ODMR^{29,57} and pulsed-ODMR).^{4,5,44,55} The black diamonds show NV-center all-optical thermometries.^{58–61} The black circles show GeV⁻-center all-optical thermometries.^{52–54} The black triangles show SiV⁻-all-optical thermometries.^{48,51,56} The black down-pointing triangle shows the tinvacancy center in all-optical thermometry.⁵¹ The black double triangle shows the all-optical thermometry of an SiV⁻-GeV⁻ hybrid system.⁶² The red-filled circles show the estimated sensitivities of single GeV⁻ centers in DND.²⁵ The red-filled triangle shows the estimated sensitivity of a single SiV⁻ in a single SiV-DND.³⁰ The black-filled circle (triangle) shows the sensitivity of a single GeV⁻ (SiV⁻) center, as estimated from the result for a GeV⁻ (Ref. 53) [SiV⁻ (Ref. 48)] ensemble in bulk diamond.

ground fluorescence from SiV⁻ diminishes, thereby augmenting the relative fluorescence ratio of NV⁻ and, consequently, enhancing the ODMR contrast. This phenomenon suggests that the ODMR contrast could be further improved using a short-pass filter near the ZPL of SiV⁻, effectively reducing the SiV⁻ fluorescence during the cw-ODMR measurements and further enhancing the sensitivity of ODMR-based techniques.

D. Temperature sensitivity

Here, we present an analysis of the correlation between the recently identified temperature sensitivity η_T and the size of diamond sensors (Fig. 4).^{4,5,25,29,30,44,48,51–62} Two major methodologies are employed in temperature sensing: ODMR-based techniques and all-optical approaches. The former utilizes the quantum characteristics of NV⁻ at room temperature, whereas the latter relies on the ZPL of color centers. In both methodologies, an increase in sensor size typically results in enhanced sensitivity. This enhancement in sensitivity is attributable to the increased number of color centers and the improved quality of these defects in larger sensors. Among the ODMR techniques, laser and microwave-pulsed ODMR methods typically demonstrate an enhancement in temperature sensitivity, with $\eta_T = 0.13$ K/ $\sqrt{\text{Hz}}$ for single 50-nm NV⁻-containing nanodiamonds⁴ and ~ 0.01 K/ $\sqrt{\text{Hz}}$ for bulk diamonds.^{4,5,44,55} Concerning all-optical techniques, the sensitivities for sensors ranging from NDs to bulk diamonds mostly lie within the range of $1 \geq \eta_T \geq 0.1$ K/ $\sqrt{\text{Hz}}$. Nonetheless, certain studies have demonstrated a high sensitivity close to 0.01 K/ $\sqrt{\text{Hz}}$ through unique measurement methodologies⁵⁴ or data analysis approaches.⁵⁶ In our case of NV⁻ in Si-DND, it is the smallest NV⁻ sensor investigated with temperature sensitivity, and it is the only hybrid SiV⁻-NV⁻ sensor to be applied to temperature sensing ever reported. Given that the particle size of the Si-DND is small and the average number of NVs⁻ per particle is substantially less than 1, the probability of multiple NV⁻ centers co-existing in a single DND particle is sufficiently low. Therefore, the estimated single NV⁻ sensitivity in Si-DND can be considered the sensitivity of a single DND particle.

IV. CONCLUSION

To conclude, we report on temperature sensing using the directly silicon-doped DNDs, which contain both temperature-responsive NV⁻ and SiV⁻. They are created efficiently during the dynamic detonation synthesis without the need for electron or ion irradiation. The ODMR signal is found to be strongly enhanced after intensive surface cleaning with boiling acid, with $\sim 50\%$ of the fluorescence spots display clear ODMR signals. The NV⁻ concentration and the particle core size are estimated to be 0.35 ppm using ESR spectroscopy and 11.2 nm using TEM, averaging 1 NV⁻ for every 22 DND particles. The temperature-dependent shifts in the cw-ODMR spectrum of NV⁻ and in the ZPL of SiV⁻ are consistent with the values reported in the literature, leading to the smallest multi-color nanodiamond thermometry ever reported. The average temperature sensitivity of the Si-DND aggregates is estimated to be 0.74 ± 0.09 K/ $\sqrt{\text{Hz}}$, and the highest temperature sensitivity is estimated to be 0.36 ± 0.01 K/ $\sqrt{\text{Hz}}$. Nonetheless, the sensitivity is expected to be further improved through optimization of measurement protocols such as using the *D*-Ramsey or further increasing the number of NVs⁻ with electron irradiation^{21,63} and annealing,^{64,65} because the sensitivity and precision of the single DND will further improve in proportion to the square root of the number of color centers. The improvement in temperature sensitivity to sub-kelvin precision is critical for living-cell measurements, including distinguishing temperature distribution differences between a nucleus and

cytoplasm¹³ and monitoring temperature changes in mitochondria after activation (~10 K increase in 20 min).⁶⁶ Finally, we demonstrate multimodal temperature sensing using both NV⁻ and SiV⁻ in the same confocal volume, suggesting their high compatibility and the potential expansion of the diamond's quantum sensing toolbox, including recently developed GeV⁻ in DND.²⁵ We believe these findings are important for the future development of brighter and more versatile ultrasmall diamond sensors.

SUPPLEMENTARY MATERIAL

The supplementary material accompanying this article provides detailed material characterization, including the methodology for particle size determination via TEM, and extensive confocal images of NV⁻ centers as shown in Fig. 2. It also includes their fluorescence intensity, individual PL and ODMR spectra, analyzes of individual temperature-induced spectral shifts, and the estimated temperature sensitivity of single NV⁻ centers. This comprehensive set of additional data supports and enriches the findings presented in the main paper.

ACKNOWLEDGMENTS

The authors are grateful for financial support from the Japanese Ministry of Education, Culture, Sports, Science and Technology (MEXT)-QLEAP Project (No. JPMXS0120330644) and a Kakenhi Grant-in-Aid (No. 21H04653) from the Japan Society for the Promotion of Science (JSPS). We would also like to express our sincere gratitude to Dr. Takuya F. Segawa for the insightful discussions and valuable suggestions.

AUTHOR DECLARATIONS

Conflict of Interest

The authors have no conflicts to disclose.

Author Contributions

Frederick T.-K. So: Data curation (equal); Formal analysis (equal); Investigation (equal); Writing – original draft (lead). **Nene Hariki:** Formal analysis (equal); Investigation (equal). **Masaya Nemoto:** Formal analysis (equal); Investigation (equal). **Alexander I. Shames:** Formal analysis (equal). **Ming Liu:** Formal analysis (supporting). **Akihiko Tsurui:** Formal analysis (supporting). **Taro Yoshikawa:** Formal analysis (supporting). **Yuto Makino:** Formal analysis (supporting). **Masanao Ohori:** Investigation (supporting). **Masanori Fujiwara:** Formal analysis (equal); Investigation (equal); Writing – original draft (equal). **Ernst David Herbschleb:** Formal analysis (supporting); Writing – review & editing (supporting). **Naoya Morioka:** Formal analysis (supporting). **Izuru Ohki:** Formal analysis (supporting). **Masahiro Shirakawa:** Formal analysis (supporting). **Ryuji Igarashi:** Formal analysis (supporting). **Masahiro Nishikawa:** Formal analysis (equal); Funding acquisition (supporting); Investigation (equal); Writing – review & editing (supporting).

Norikazu Mizuochi: Conceptualization (equal); Funding acquisition (lead); Supervision (equal); Writing – original draft (equal); Writing – review & editing (lead).

DATA AVAILABILITY

The data that support the findings of this study are available from the corresponding author upon reasonable request.

REFERENCES

- 1 A. Gruber, A. Dräbenstedt, C. Tietz, L. Fleury, J. Wrachtrup, and C. v. Borczyskowski, "Scanning confocal optical microscopy and magnetic resonance on single defect centers," *Science* **276**, 2012 (1997).
- 2 E. D. Herbschleb, H. Kato, Y. Maruyama, T. Danjo, T. Makino, S. Yamasaki, I. Ohki, K. Hayashi, H. Morishita, M. Fujiwara, and N. Mizuochi, "Ultra-long coherence times amongst room-temperature solid-state spins," *Nat. Commun.* **10**(1), 3766 (2019).
- 3 D. D. Awschalom, R. Hanson, J. Wrachtrup, and B. B. Zhou, "Quantum technologies with optically interfaced solid-state spins," *Nat. Photonics* **12**(9), 516–527 (2018).
- 4 P. Neumann, I. Jakobi, F. Dolde, C. Burk, R. Reuter, G. Waldherr, J. Honert, T. Wolf, A. Brunner, J. H. Shim, D. Suter, H. Sumiya, J. Isoya, and J. Wrachtrup, "High-precision nanoscale temperature sensing using single defects in diamond," *Nano Lett.* **13**(6), 2738–2742 (2013).
- 5 G. Kucsko, P. C. Maurer, N. Y. Yao, M. Kubo, H. J. Noh, P. K. Lo, H. Park, and M. D. Lukin, "Nanometre-scale thermometry in a living cell," *Nature* **500**(7460), 54–58 (2013).
- 6 R. Igarashi, T. Sugi, S. Sotoma, T. Genjo, Y. Kumiya, E. Walinda, H. Ueno, K. Ikeda, H. Sumiya, H. Tochio, Y. Yoshinari, Y. Harada, and M. Shirakawa, "Tracking the 3D rotational dynamics in nanoscopic biological systems," *J. Am. Chem. Soc.* **142**, 7542–7554 (2020).
- 7 F. Dolde, H. Fedder, M. W. Doherty, T. Nöbauer, F. Rempp, G. Balasubramanian, T. Wolf, F. Reinhard, L. C. L. Hollenberg, F. Jelezko, and J. Wrachtrup, "Electric-field sensing using single diamond spins," *Nat. Phys.* **7**, 459–463 (2011).
- 8 X. Wang, J. Xu, S. Ge, L. Zou, D. Sang, J. Fan, and Q. Wang, "Recent applications of nanodiamond quantum biosensors: A review," *APL Mater.* **11**(9), 090603 (2023).
- 9 A. Mzyk, A. Sigaeva, and R. Schirhagl, "Relaxometry with nitrogen vacancy (NV) centers in diamond," *Acc. Chem. Res.* **55**(24), 3572–3580 (2022).
- 10 B. S. Miller, L. Bezinge, H. D. Gliddon, D. Huang, G. Dold, E. R. Gray, J. Heaney, P. J. Dobson, E. Nastouli, J. J. L. Morton, and R. A. McKendry, "Spin-enhanced nanodiamond biosensing for ultrasensitive diagnostics," *Nature* **587**(7835), 588–593 (2020).
- 11 S. Sotoma, C. Zhong, J. C. Y. Kah, H. Yamashita, T. Plakhotnik, Y. Harada, and M. Suzuki, "In situ measurements of intracellular thermal conductivity using heater-thermometer hybrid diamond nanosensors," *Sci. Adv.* **7**(3), eabd7888 (2021).
- 12 B. B. Lowell and B. M. Spiegelman, "Towards a molecular understanding of adaptive thermogenesis," *Nature* **404**(6778), 652–660 (2000).
- 13 K. Okabe, N. Inada, C. Gota, Y. Harada, T. Funatsu, and S. Uchiyama, "Intracellular temperature mapping with a fluorescent polymeric thermometer and fluorescence lifetime imaging microscopy," *Nat. Commun.* **3**, 705 (2012).
- 14 S. L. Keller, W. H. Pitcher, W. H. Huestis, and H. M. Mc Connell, "Red blood cell lipids form immiscible liquids," *Phys. Rev. Lett.* **81**(22), 5019–5022 (1998).
- 15 S. L. Veatch, P. Cicuta, P. Sengupta, A. Honerkamp-Smith, D. Holowka, and B. Baird, "Critical fluctuations in plasma membrane vesicles," *ACS Chem. Biol.* **3**(5), 287–293 (2008).
- 16 K. M. McCabe and M. Hernandez, "Molecular thermometry," *Pediatr. Res.* **67**(5), 469–475 (2010).
- 17 R. Schirhagl, K. Chang, M. Loretz, and C. L. Degen, "Nitrogen-vacancy centers in diamond: Nanoscale sensors for physics and biology," *Annu. Rev. Phys. Chem.* **65**(1), 83–105 (2014).

- ¹⁸S. Sotoma, D. Terada, T. F. Segawa, R. Igarashi, Y. Harada, and M. Shirakawa, "Enrichment of ODMR-active nitrogen-vacancy centres in five-nanometre-sized detonation-synthesized nanodiamonds: Nanoprobes for temperature, angle and position," *Sci. Rep.* **8**(1), 5463 (2018).
- ¹⁹A. Sigaeva, A. Hochstetter, S. Bouyim, M. Chipaux, M. Stejfova, P. Cigler, and R. Schirhagl, "Single-particle tracking and trajectory analysis of fluorescent nanodiamonds in cell-free environment and live cells," *Small* **18**(39), 2201395 (2022).
- ²⁰M. Chipaux, K. J. van der Laan, S. R. Hemelaar, M. Hasani, T. Zheng, and R. Schirhagl, "Nanodiamonds and their applications in cells," *Small* **14**(24), 1704263 (2018).
- ²¹F. T. K. So, A. I. Shames, D. Terada, T. Genjo, H. Morishita, I. Ohki, T. Ohshima, S. Onoda, H. Takashima, S. Takeuchi, N. Mizuochi, R. Igarashi, M. Shirakawa, and T. F. Segawa, "Anomalous formation of irradiation-induced nitrogen-vacancy centers in 5 nm-sized detonation nanodiamonds," *J. Phys. Chem. C* **126**(11), 5206–5217 (2022).
- ²²D. Terada, F. T. K. So, B. Hattendorf, T. Yanagi, E. Ōsawa, N. Mizuochi, M. Shirakawa, R. Igarashi, and T. F. Segawa, "A simple and soft chemical deaggregation method producing single-digit detonation nanodiamonds," *Nanoscale Adv.* **4**(10), 2268–2277 (2022).
- ²³V. Y. Dolmatov, "Detonation synthesis ultradispersed diamonds: Properties and applications," *Russ. Chem. Rev.* **70**(7), 607–626 (2001).
- ²⁴D. Terada, T. F. Segawa, A. I. Shames, S. Onoda, T. Ohshima, E. Ōsawa, R. Igarashi, and M. Shirakawa, "Monodisperse five-nanometer-sized detonation nanodiamonds enriched in nitrogen-vacancy centers," *ACS Nano* **13**(6), 6461–6468 (2019).
- ²⁵M. Fujiwara, H. Fu, N. Hariki, I. Ohki, Y. Makino, M. Liu, A. Tsurui, T. Yoshikawa, M. Nishikawa, and N. Mizuochi, "Germanium-vacancy centers in detonation nanodiamond for all-optical nanoscale thermometry," *Appl. Phys. Lett.* **123**(18), 181903 (2023).
- ²⁶Y. Makino, T. Yoshikawa, A. Tsurui, M. Liu, G. Yamagishi, M. Nishikawa, T. Mahiko, M. Ohno, M. Ashida, and N. Okuyama, "Direct synthesis of group IV-vacancy center-containing nanodiamonds via detonation process using aromatic compound as group IV element source," *Diamond Relat. Mater.* **130**, 109493 (2022).
- ²⁷Y. Makino, T. Mahiko, M. Liu, A. Tsurui, T. Yoshikawa, S. Nagamachi, S. Tanaka, K. Hokamoto, M. Ashida, M. Fujiwara, N. Mizuochi, and M. Nishikawa, "Straightforward synthesis of silicon vacancy (SiV) center-containing single-digit nanometer nanodiamonds via detonation process," *Diamond Relat. Mater.* **112**, 108248 (2021).
- ²⁸S. L. Y. Chang, P. Reineck, A. Krueger, and V. N. Mochalin, "Ultrasml nanodiamonds: Perspectives and questions," *ACS Nano* **16**(6), 8513–8524 (2022).
- ²⁹M. Fujiwara and Y. Shikano, "Diamond quantum thermometry: From foundations to applications," *Nanotechnology* **32**(48), 482002 (2021).
- ³⁰M. Fujiwara, G. Uchida, I. Ohki, M. Liu, A. Tsurui, T. Yoshikawa, M. Nishikawa, and N. Mizuochi, "All-optical nanoscale thermometry based on silicon-vacancy centers in detonation nanodiamonds," *Carbon* **198**, 57–62 (2022).
- ³¹R. Weissleder, "A clearer vision for *in vivo* imaging," *Nat. Biotechnol.* **19**(4), 316–317 (2001).
- ³²W. Liu, M. N. A. Alam, Y. Liu, V. N. Agafonov, H. Qi, K. Koynov, V. A. Davydov, R. Uzbekov, U. Kaiser, T. Lasser, F. Jelezko, A. Ermakova, and T. Weil, "Silicon-vacancy nanodiamonds as high performance near-infrared emitters for live-cell dual-color imaging and thermometry," *Nano Lett.* **22**(7), 2881–2888 (2022).
- ³³S. Sajedi, H. Sabet, and H. S. Choi, "Intraoperative biophotonic imaging systems for image-guided interventions," *Nanophotonics* **8**(1), 99–116 (2018).
- ³⁴Y. Makino, Y. Saito, H. Takehara, A. Tsurui, N. Okuyama, and M. Ashida, "Effect of particle size on the optical properties of silicon-vacancy centers in nanodiamonds fabricated by a detonation process," *Phys. Status Solidi A* **219**(22), 2200342 (2022).
- ³⁵A. I. Shames, V. Yu Osipov, H. J. Von Bardeleben, and A. Ya Vul, "Spin $S = 1$ centers: A universal type of paramagnetic defects in nanodiamonds of dynamic synthesis," *J. Phys.: Condens. Matter* **24**(22), 225302 (2012).
- ³⁶A. I. Shames, V. Y. Osipov, H. J. Von Bardeleben, J. P. Boudou, F. Treussart, and A. Y. Vul, "Native and induced triplet nitrogen-vacancy centers in nano- and micro-diamonds: Half-field electron paramagnetic resonance fingerprint," *Appl. Phys. Lett.* **104**(6), 063107 (2014).
- ³⁷T. F. Segawa and A. I. Shames, "How to identify, attribute, and quantify triplet defects in ensembles of small nanoparticles," *J. Phys. Chem. Lett.* **11**(17), 7438–7442 (2020).
- ³⁸A. I. Shames, A. Dalis, A. D. Greentree, B. C. Gibson, H. Abe, T. Ohshima, O. Shenderova, A. Zaitsev, and P. Reineck, "Near-infrared fluorescence from silicon- and nickel-based color centers in high-pressure high-temperature diamond micro- and nanoparticles," *Adv. Opt. Mater.* **8**(23), 2001047 (2020).
- ³⁹V. Y. Osipov, A. I. Shames, T. Enoki, K. Takai, M. Baidakova, and A. Y. Vul, "Paramagnetic defects and exchange coupled spins in pristine ultrananocrystalline diamonds," *Diamond Relat. Mater.* **16**, 2035–2038 (2007).
- ⁴⁰P. Reineck, D. W. M. Lau, E. R. Wilson, K. Fox, M. R. Field, C. Deeepojananan, V. N. Mochalin, and B. C. Gibson, "Effect of surface chemistry on the fluorescence of detonation nanodiamonds," *ACS Nano* **11**(11), 10924–10934 (2017).
- ⁴¹X. D. Chen, C. H. Dong, F. W. Sun, C. L. Zou, J. M. Cui, Z. F. Han, and G. C. Guo, "Temperature dependent energy level shifts of nitrogen-vacancy centers in diamond," *Appl. Phys. Lett.* **99**(16), 161903 (2011).
- ⁴²V. M. Acosta, E. Bauch, M. P. Ledbetter, A. Waxman, L. S. Bouchard, and D. Budker, "Temperature dependence of the nitrogen-vacancy magnetic resonance in diamond," *Phys. Rev. Lett.* **104**(7), 070801 (2010).
- ⁴³E. Bauch, S. Singh, J. Lee, C. A. Hart, J. M. Schloss, M. J. Turner, J. F. Barry, L. M. Pham, N. Bar-Gill, S. F. Yelin, and R. L. Walsworth, "Decoherence of ensembles of nitrogen-vacancy centers in diamond," *Phys. Rev. B* **102**(13), 134210 (2020).
- ⁴⁴D. M. Toyli, C. F. De Las Casas, D. J. Christle, V. V. Dobrovitski, and D. D. Awschalom, "Fluorescence thermometry enhanced by the quantum coherence of single spins in diamond," *Proc. Natl. Acad. Sci. U. S. A.* **110**(21), 8417–8421 (2013).
- ⁴⁵S. Dhomkar, H. Jayakumar, P. R. Zangara, and C. A. Meriles, "Charge dynamics in near-surface, variable-density ensembles of nitrogen-vacancy centers in diamond," *Nano Lett.* **18**(6), 4046–4052 (2018).
- ⁴⁶B. A. Myers, A. Ariyaratne, and A. B. Jayich, "Double-quantum spin-relaxation limits to coherence of near-surface nitrogen-vacancy centers," *Phys. Rev. Lett.* **118**(19), 197201 (2017).
- ⁴⁷M. Kim, H. J. Mamin, M. H. Sherwood, K. Ohno, D. D. Awschalom, and D. Rugar, "Decoherence of near-surface nitrogen-vacancy centers due to electric field noise," *Phys. Rev. Lett.* **115**(8), 087602 (2015).
- ⁴⁸C. T. Nguyen, R. E. Evans, A. Sipahigil, M. K. Bhaskar, D. D. Sukachev, V. N. Agafonov, V. A. Davydov, L. F. Kulikova, F. Jelezko, and M. D. Lukin, "All-optical nanoscale thermometry with silicon-vacancy centers in diamond," *Appl. Phys. Lett.* **112**(20), 203102 (2018).
- ⁴⁹G. Q. Liu, X. Feng, N. Wang, Q. Li, and R. B. Liu, "Coherent quantum control of nitrogen-vacancy center spins near 1000 kelvin," *Nat. Commun.* **10**(1), 1344 (2019).
- ⁵⁰M. Zaghrioui, V. N. Agafonov, and V. A. Davydov, "Nitrogen and group-IV (Si, Ge) vacancy color centres in nano-diamonds: Photoluminescence study at high temperature (25 °C–600 °C)," *Mater. Res. Express* **7**(1), 015043 (2020).
- ⁵¹M. Alkahtani, I. Cojocar, X. Liu, T. Herzig, J. Meijer, J. Küpper, T. Lühmann, A. V. Akimov, and P. R. Hemmer, "Tin-vacancy in diamonds for luminescent thermometry," *Appl. Phys. Lett.* **112**(24), 241902 (2018).
- ⁵²T. T. Tran, B. Regan, E. A. Ekimov, Z. Mu, Y. Zhou, W. Gao, P. Narang, A. S. Solntsev, M. Toth, I. Aharonovich, and C. Bradac, "Anti-Stokes excitation of solid-state quantum emitters for nanoscale thermometry," in *2019 Conference on Lasers and Electro-Optics, CLEO 2019—Proceedings* (IEEE, 2019), pp. 1–7.
- ⁵³J. W. Fan, I. Cojocar, J. Becker, I. V. Fedotov, M. H. A. Alkahtani, A. Alajlan, S. Blakley, M. Rezaee, A. Lyamkina, Y. N. Palyanov, Y. M. Borzdov, Y. P. Yang, A. Zheltikov, P. Hemmer, and A. V. Akimov, "Germanium-vacancy color center in diamond as a temperature sensor," *ACS Photonics* **5**(3), 765–770 (2018).
- ⁵⁴S. Blakley, X. Liu, I. Fedotov, I. Cojocar, C. Vincent, M. Alkahtani, J. Becker, M. Kieschnick, T. Lühmann, J. Meijer, P. Hemmer, A. Akimov, M. Scully, and A. Zheltikov, "Fiber-optic quantum thermometry with germanium-vacancy centers in diamond," *ACS Photonics* **6**(7), 1690–1693 (2019).
- ⁵⁵J. Wang, F. Feng, J. Zhang, J. Chen, Z. Zheng, L. Guo, W. Zhang, X. Song, G. Guo, L. Fan, C. Zou, L. Lou, W. Zhu, and G. Wang, "High-sensitivity temperature sensing using an implanted single nitrogen-vacancy center array in diamond," *Phys. Rev. B* **91**(15), 155404 (2015).

- ⁵⁶S. Choi, V. N. Agafonov, V. A. Davydov, and T. Plakhotnik, "Ultrasensitive all-optical thermometry using nanodiamonds with a high concentration of silicon-vacancy centers and multiparametric data analysis," *ACS Photonics* **6**(6), 1387–1392 (2019).
- ⁵⁷Y. K. Tzeng, P. C. Tsai, H. Y. Liu, O. Y. Chen, H. Hsu, F. G. Yee, M. S. Chang, and H. C. Chang, "Time-resolved luminescence nanothermometry with nitrogen-vacancy centers in nanodiamonds," *Nano Lett.* **15**(6), 3945–3952 (2015).
- ⁵⁸T. Plakhotnik, M. W. Doherty, J. H. Cole, R. Chapman, and N. B. Manson, "All-optical thermometry and thermal properties of the optically detected spin resonances of the NV-center in nanodiamond," *Nano Lett.* **14**(9), 4989–4996 (2014).
- ⁵⁹T. Plakhotnik, H. Aman, and H. C. Chang, "All-optical single-nanoparticle ratiometric thermometry with a noise floor of $0.3 \text{ K Hz}^{-1/2}$," *Nanotechnology* **26**(24), 245501 (2015).
- ⁶⁰P. C. Tsai, C. P. Epperla, J. S. Huang, O. Y. Chen, C. C. Wu, and H. C. Chang, "Measuring nanoscale thermostability of cell membranes with single gold–diamond nanohybrids," *Angew. Chem., Int. Ed.* **56**(11), 3025–3030 (2017).
- ⁶¹Y. Y. Hui, O. Y. Chen, T. Azuma, B. M. Chang, F. J. Hsieh, and H. C. Chang, "All-optical thermometry with nitrogen-vacancy centers in nanodiamond-embedded polymer films," *J. Phys. Chem. C* **123**, 15366–15374 (2019).
- ⁶²Y. Chen, C. Li, T. Yang, E. A. Ekimov, C. Bradac, S. T. Ha, M. Toth, I. Aharonovich, and T. T. Tran, "Real-time ratiometric optical nanoscale thermometry," *ACS Nano* **17**(3), 2725–2736 (2023).
- ⁶³S. Sotoma, Y. Yoshinari, R. Igarashi, A. Yamazaki, S. H. Yoshimura, H. Tochio, M. Shirakawa, and Y. Harada, "Effective production of fluorescent nanodiamonds containing negatively-charged nitrogen-vacancy centers by ion irradiation," *Diamond Relat. Mater.* **49**, 33–38 (2014).
- ⁶⁴K. Shimazaki, H. Kawaguchi, H. Takashima, T. F. Segawa, F. T. K. So, D. Terada, S. Onoda, T. Ohshima, M. Shirakawa, and S. Takeuchi, "Fabrication of detonation nanodiamonds containing silicon-vacancy color centers by high temperature annealing," *Phys. Status Solidi A* **218**(19), 2100144 (2021).
- ⁶⁵M. Capelli, A. H. Heffernan, T. Ohshima, H. Abe, J. Jeske, A. Hope, A. D. Green-tree, P. Reineck, and B. C. Gibson, "Increased nitrogen-vacancy centre creation yield in diamond through electron beam irradiation at high temperature," *Carbon* **143**, 714–719 (2019).
- ⁶⁶D. Chrétien, P. Bénil, H.-H. Ha, S. Keipert, R. El-Khoury, Y.-T. Chang, M. Jastroch, H. T. Jacobs, P. Rustin, and M. Rak, "Mitochondria are physiologically maintained at close to 50°C ," *PLoS Biol.* **16**(1), e2003992 (2018).